Hydrazine Formation via Ni^{III}-NH_2 Radical Coupling in Ni-Mediated Ammonia Oxidation

Nina X. Gu, Paul H. Oyala, and Jonas C. Peters*

ABSTRACT

Given the diverse mechanistic possibilities for the overall $6e^-/6H^+$ transformation of ammonia to dinitrogen, identification of $M(NH_x)$ intermediates involved in N–N bond formation is a central mechanistic challenge. In analogy to water oxidation mechanisms, which widely invoke metal oxo intermediates, metal imide and nitride intermediates have commonly been proposed for ammonia oxidation, and stoichiometric demonstration of N–N bond formation from these metal-ligand multiply bonded species is well-precedented. In contrast, while the homocoupling of M–NH_2 species to form hydrazine has been hypothesized as the key N–N bond forming step in certain molecular ammonia oxidation systems, well-defined examples of this transformation from M–NH_2 complexes are essentially without precedent. This work reports the first example of net ammonia oxidation mediated by a molecular Ni species, a transformation carried out via formal Ni^{II}/Ni^{III} oxidation states. The available data are consistent with a Ni^{III}–NH_2 intermediate featuring substantial spin at N undergoing N–N bond formation to generate a $Ni^{II}_2(N_2H_4)$ complex. Additional and structurally unusual $Ni_x(N_yH_z)$ species – including a $Ni_2(trans$-$N_2H_2)$ complex – are characterized and studied as intermediates in the Ni-mediated ammonia oxidation cycle described herein.

INTRODUCTION

Ammonia (NH_3) offers attractive opportunities for energy storage and use, for example as a hydrogen fuel carrier or as a combustible, energy-dense fuel.[1] For such applications, catalysts that mediate the $6e^-/6H^+$ conversion of ammonia to N_2 are key and have been the subject of many studies.[2] Well-defined molecular model systems are amenable to detailed mechanistic interrogation, and their study in this context is expanding rapidly. Stoichiometric ammonia oxidation (AO) to N_2 has been demonstrated for transition metal complexes of Mo,[3] Mn,[4] Os,[5] and Ru.[6,7] More recently, AO catalysis has been reported using Ru[8] and Fe[9] complexes under chemical and electrochemical conditions.

Several of these molecular catalyst systems (or closely-related derivatives) can also mediate related $4e^-/4H^+$ water oxidation catalysis (WOC) to liberate O_2,[10] raising the question as to whether ammonia and water oxidation proceed through conceptually related pathways. For WOC, the intermediacy of metal oxo species are often implicated, and O–O bond formation is posited to occur via bimolecular oxo coupling or nucleophilic attack of a metal oxo intermediate by H_2O (Fig. 1).[11,12]

Water Oxidation: *Common Pathways for O–O Bond Formation*

Ammonia Oxidation: *Common Pathways for N–N Bond Formation*

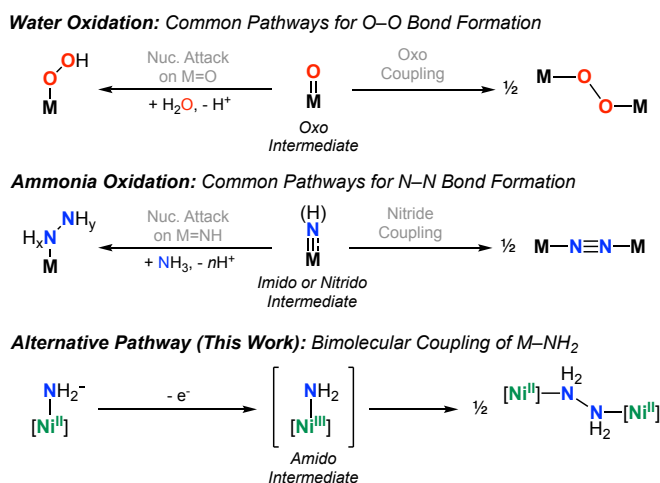**Alternative Pathway (This Work):** *Bimolecular Coupling of M–NH₂*

Figure 1. (top) Proposed pathways for O–O bond formation in water oxidation catalysis (charges not specified) (middle) Proposed pathways for N–N bond formation in ammonia oxidation catalysis (charges not specified) (bottom) Proposed N–N coupling pathway discussed in this work from a Ni–NH$_2$ species

In analogy to WOC, intermediates featuring metal-to-nitrogen multiple bonds (specifically, metal nitride and imide intermediates) have been proposed for several systems that mediate stoichiometric or catalytic ammonia oxidation.[3,4abd,5abd,6ab,8ac] Furthermore, bimolecular nitride (M≡N)[4ab,5b,13] and imide (M=NR)[14] coupling, and the nucleophilic attack of amines on terminal imides[5d,8a,15] and nitrides,[16] have been implicated in relevant N–N bond forming reactions.

In contrast, well-defined examples of N–N bond formation through bimolecular coupling of parent metal-amide intermediates (M–NH$_2$) are lacking, despite such coupling having been recently hypothesized in catalytic ammonia oxidation mediated by (tetramesitylporphyrin)Ru(NH$_3$)$_2$.[8d] The conceptually related reductive elimination of an N−N single bond from M−NR$_2$[17,18] and M−N=R[19] species have also been demonstrated, although such examples are likewise uncommon.

Pertinent to M–NH$_2$ coupling, Collman and coworkers reported that treatment of a cofacial {(porphyrin)Ru(NH$_3$)}$_2$ complex with either tBuOOH or an oxidant with base afforded a mixture of Ru$_2$(N$_2$H$_4$), Ru$_2$(N$_2$H$_2$), and Ru$_2$(N$_2$) species as the N–N coupled products. The authors hypothesized hy-

drazine formation to occur via coupling of two unobserved $Ru^{III}–NH_2$ fragments.[5d] Relatedly, Sellmann and coworkers detected trace $CpMn(CO)_2(N_2H_4)$ from bulk electrochemical oxidation experiments with $CpMn(CO)_2NH_3$,[3c] again suggesting a possible role for an unobserved $Mn–NH_2$ intermediate.[5d]

Ammonia oxidation pathways that access N–N bond formation at the amide state may potentially traverse a narrower catalyst redox range compared to those involving higher-valent imide or nitride intermediates. In turn, such a pathway may provide a viable strategy for late transition metal complexes to mediate the multielectron AO process, given that metal-ligand multiple bonded moieties are generally less accessible in transition metals beyond Group 8 compared to earlier metals.[20]

As part of our interest in exploring mid-to-late first row metals for AO catalysis,[9] we report here on studies of a nickel system that mediates stepwise NH_3 oxidation. A reactive $Ni^{III}–NH_2$ species is proposed as a key intermediate en route to hydrazine formation via bimolecular reductive elimination to form dinickel $Ni^{II}_2(N_2H_4)$ complex; the latter species can facilitate further N_xH_y oxidation to ultimately yield ammonia-derived dinitrogen.

RESULTS AND DISCUSSION

Our group recently reported the synthesis of the tetradentate bis(phosphino)(thiolato)silyl ligand $(HSiP_2S^{iPr})$[21] and the nickel-bound species, $[(SiP_2S)Ni]_2(N_2)$ (**1**).[22,23] Treatment of **1** with a THF solution of ammonia provides $(SiP_2S)Ni^{II}(NH_3)$ (**2**). Deprotonation of the coordinated NH_3 ligand with nBuLi in THF affords $[(SiP_2S)Ni^{II}(NH_2)]Li$ (**3**), which can also be prepared by treatment of **1** with $LiNH_2$ in THF (Scheme 1, Fig. 2A). ^1H NMR data in C_6D_6 of **3** demonstrate the coordination of three THF molecules to the lithium cation,[24] and recrystallization in benzene allows structural characterization of the solvent-free derivative as a dimer, $[(SiP_2S)Ni^{II}NH_2]_2Li_2$ (Fig. 2B). Nickel complexes featuring a terminal NH_2 ligand are relatively uncommon, and to our knowledge, reported examples are limited to four-coordinate, pincer-ligated Ni^{II} species.[25]
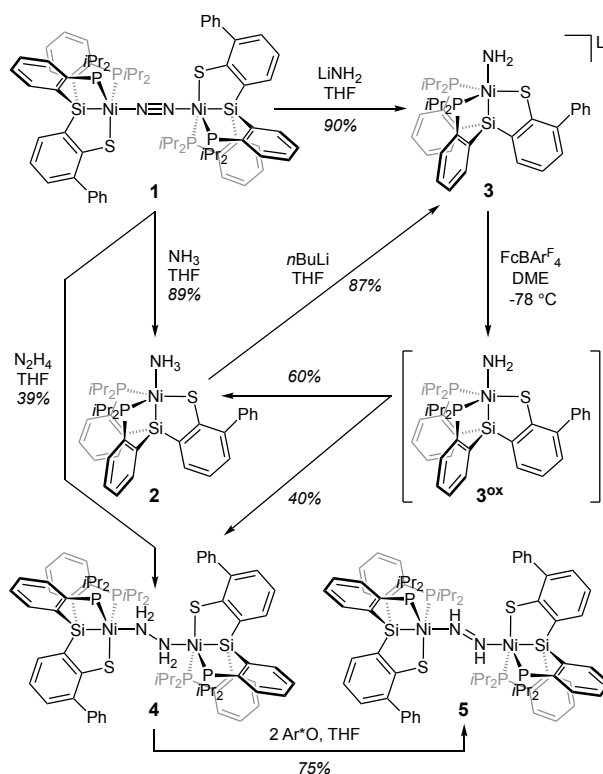
Scheme 1. Synthesis of compounds **2-5**. Ar*O = 2,4,6-tri-*ter*t-butylphenoxyl radical

The cyclic voltammogram of **3** with 0.4 M [NBu₄][PF₆] in THF reveals an oxidation event at -0.72 V vs. Cp₂Fe/Cp₂Fe⁺, corresponding to its formal Ni^{II}/Ni^{III} couple. The reaction of **3** with one equivalent of [Cp₂Fe][BAr$^F_4$] (BAr$^F_4$ = B(3,5-(CF₃)₂C₆H₃)₄) at -78 °C in 1,2-dimethoxyethane (DME) regenerates its precursor ammonia adduct **2** in *ca.* 60% yield.[26] Relatedly, our group had previously observed that the oxidation of an Fe^{II}–NH₂ complex led to the corresponding Fe^{II}–NH₃ species, possibly due to hydrogen atom abstraction from solvent by a transient Fe^{III}–NH₂ intermediate.[27] Most interesting is the observation of an N–N coupled hydrazine product, [(SiP₂S)Ni^{II}]₂(N₂H₄) (**4**, *ca.* 40% yield) in the reaction mixture. Of note, neither H₂ nor free NH₃ are detected as products in this oxidation reaction. Complex **4** can be independently generated via treatment of the N₂-adduct **1** with hydrazine. Its solid-state structure reveals an N–N bond length of 1.488(4) Å, slightly elongated compared to free hydrazine (1.449 Å, Fig. 2C).[28] Oxidation of the ¹⁵N-labeled and ²H-labeled derivatives of **3**, [(SiP₂S)Ni^{II}(¹⁵NH₂)]Li and [(SiP₂S)Ni^{II}(ND₂)]Li, respectively, affords the corresponding [(SiP₂S)Ni^{II}]₂(¹⁵N₂H₄) and [(SiP₂S)Ni^{II}]₂(N₂D₄) complexes as the N–N coupled products, confirming that the coordinated hydrazine fragment is exclusively amide-derived (Fig. 3).[29]
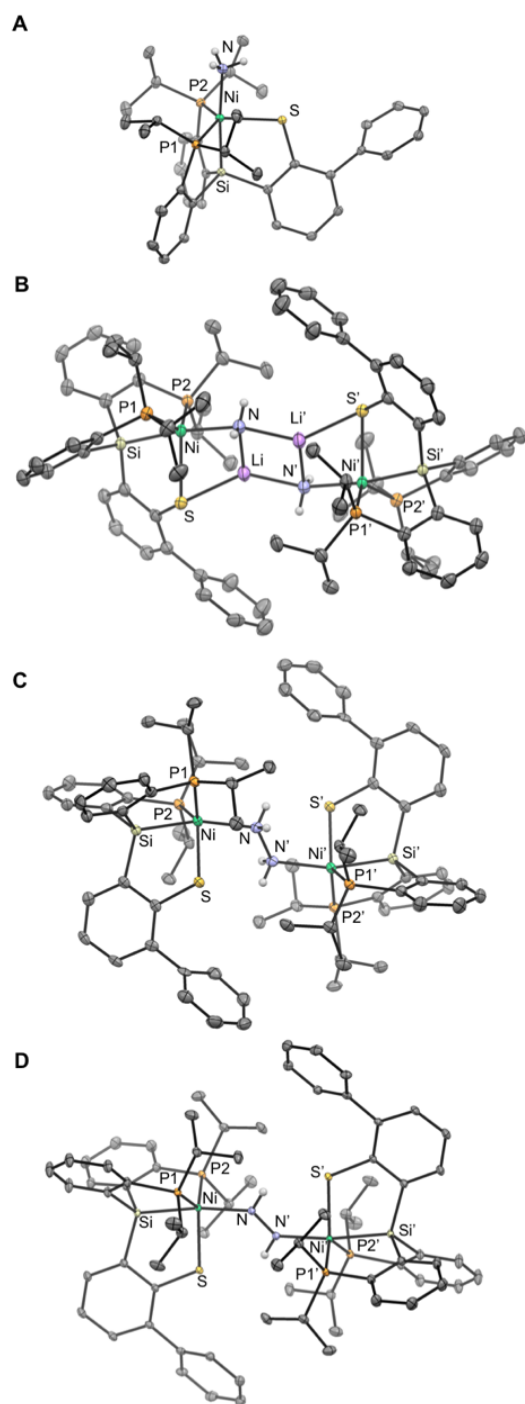
Figure 2. Crystal structures of compounds (A) **2**, (B) **3**, (C) **4**, and (D) **6**. Solvent molecules, disordered components, and C-*H* hydrogens omitted for clarity. Ellipsoids shown at 50% probability.
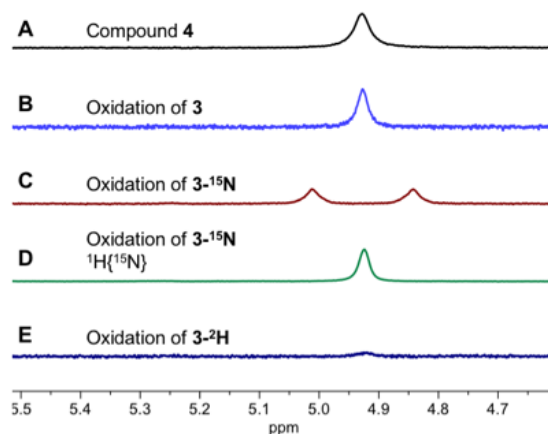
Figure 3. Partial ^{1}H NMR spectra showing the resonance at 4.93 ppm (corresponding to the 4 N-*H* protons) of (A) compound **4** generated by treatment of **1** with N_2H_4 and (B-E) reaction mixtures generated by oxidation of isotopologues of **3** in DME (C_6D_6, 400 MHz, 298 K)

The observation of a substantial amount of hydrazine via the oxidation of the nickel(II) amide **3** suggests a direct role for a $Ni^{III}(NH_2)$ species in the N–N coupling step. Considering that N–N coupling is triggered by the addition of oxidant, one mechanistic possibility is that N–N bond formation occurs by the reaction of two molecules of $(SiP_2S)Ni^{III}(NH_2)$ (**3^{ox}**). Alternatively, a reaction between **3^{ox}** and **3** to form a monoanion, $\{[(SiP_2S)Ni]_2(N_2H_4)\}^-$, followed its one-electron oxidation, leads to the same product. We disfavor the latter scenario as we observe that treatment of **3** with 0.5 equivalents of $[Cp_2Fe][BAr^F_4]$ in DME at -78 °C fails to generate an EPR-active species (as would be expected for $\{[(SiP_2S)Ni]_2(N_2H_4)\}^-$). Furthermore, the one-electron reduced congener of **4** is a mixed-valent Ni^I/Ni^{II} species with the Ni^I center bearing 19 e$^-$, and thus likely an unstable, high-energy species. This argument is consistent with the electrochemistry data on **4** collected in 0.4 M $[NBu_4][PF_6]$ in THF at 25 °C, which reveals an irreversible reduction event with an onset at *ca.* -3 V vs. Fc/Fc$^+$.

We thus favor a mechanism for N–N coupling where two Ni^{III}–NH_2 fragments directly generate the hydrazine adduct **4**; the competing generation of **2** following the oxidation of **3** is presumed to arise from hydrogen-atom abstraction of DME solvent by Ni^{III}–NH_2. Consistent with this mechanistic proposal, carrying out the oxidation reaction of **3-^{2}H** in DME with twenty-fold dilution results in near quantitative formation of the amine product, $(SiP_2S)Ni^{II}(ND_2H)$, and ^{1}H NMR spectroscopy confirms the presence of the N–*H* proton. Only trace amounts of the N–N coupled hydrazine adduct are generated under these conditions.

6

It is useful to compare this mechanistic picture with a previous study from our lab, where we demonstrated that the same SiP$_2$S ligand could support a structurally related Ni^{III}–H species that undergoes release of H$_2$.[22] This step was posited to occur via a transition state featuring direct H–H coupling between two Ni^{III}–H fragments, in analogy to the proposed N–N coupling pathway proposed here (Fig. 4).
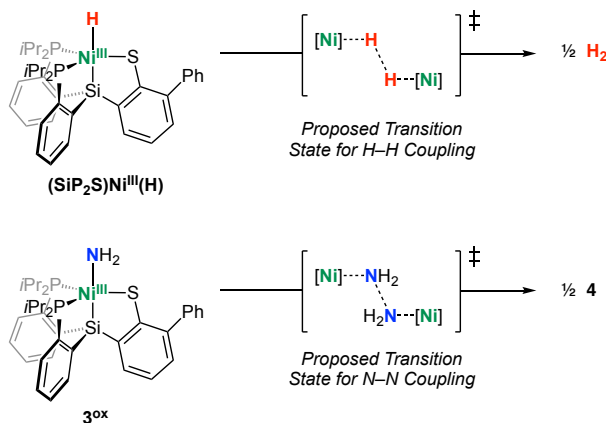

Figure 4. Comparison of proposed H–H and N–N bond formation by (SiP$_2$S)Ni^{III}X species (X = H, NH$_2$)

Attempts to spectroscopically observe **3^{ox}** in situ by oxidation of **3** with [Cp$_2$Fe][BAr$^F_4$] were unsuccessful.[30,31] However, we find that small quantities of an $S = \frac{1}{2}$ Ni^{III}-NH$_2$ can be generated by hydrogen atom abstraction from (SiP$_2$S)Ni^{II}(NH$_3$) **2** with 2,4,6-tri-*ter*t-butylphenoxyl radical in 2-MeTHF, as observed by 77 K CW EPR spectroscopy (Fig. 5A).[32] Based on variable temperature UV-vis data, the hydrogen atom abstraction of **2** by 2,4,6-tri-*ter*t-butylphenoxyl radical in 2-MeTHF is more favorable at lower temperatures; new features at 670 nm and 870 nm grow in upon cooling the solution from -78 ℃ to -130 ℃.[33] This transformation is reversible upon warming the solution, which results in the regeneration of the starting **2** and 2,4,6-tri-*ter*t-butylphenoxyl radical, demonstrating that this process is in equilibrium. Given the significantly increased stability of the observed Ni(III) amide compared to in situ-generated **3^{ox}**, we propose that treatment of 2,4,6-tri-*ter*t-butylphenoxyl radical with the amine complex **2** results in a Ni(III) amide stabilized by hydrogen bonding to 2,4,6-tri-*ter*t-butylphenol ((SiP$_2$S)Ni^{III}–NH$_2$···H–OAr, **3$^{ox'}$**, Eq. 1). Such a scenario rationalizes the observation that **3$^{ox'}$** formation is favorable at lower temperatures, due to the entropic penalties associated with formation of the hydrogen-bond stabilized amide species.

$$\mathbf{2} \;+\; \ce{[phenoxy radical]} \quad \underset{T\uparrow}{\overset{T\downarrow}{\rightleftharpoons}} \quad \mathbf{3^{ox'}} \tag{1}$$
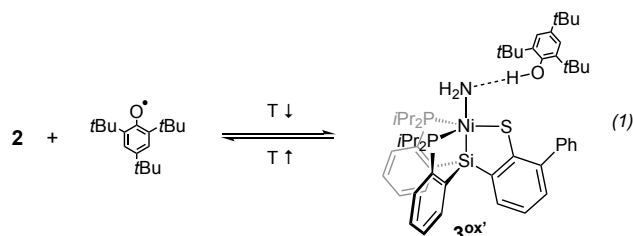
Due to this observed equilibrium, although EPR samples of $\mathbf{3^{ox'}}$ were prepared with a substoichiometric amount of organic radical compared to $\mathbf{2}$, unreacted phenoxy radical was invariably observed in the EPR spectrum, in addition to a rhombic signal attributed to $\mathbf{3^{ox'}}$ (g = [2.223, 2.084, 2.027], Table 1).[34] Preparation of the analogous ^{15}N- and ^{2}H-labeled species ($\mathbf{3^{ox'}}$-^{15}N and $\mathbf{3^{ox'}}$-^{2}H) from $(SiP_2S)Ni^{II}(^{15}NH_3)$ and $(SiP_2S)Ni^{II}(ND_3)$, respectively, yielded near identical CW EPR spectra to that of the unlabeled sample, $\mathbf{3^{ox'}}$ (Figure 5A). Nonetheless, consistent with its assignment as a Ni^{III}-NH_2 species, pulse EPR data on $\mathbf{3^{ox'}}$, $\mathbf{3^{ox'}}$-^{15}N, $\mathbf{3^{ox'}}$-^{2}H are able to definitively resolve hyperfine couplings to one isotopically sensitive nitrogen and two isotopically sensitive hydrogen nuclei.

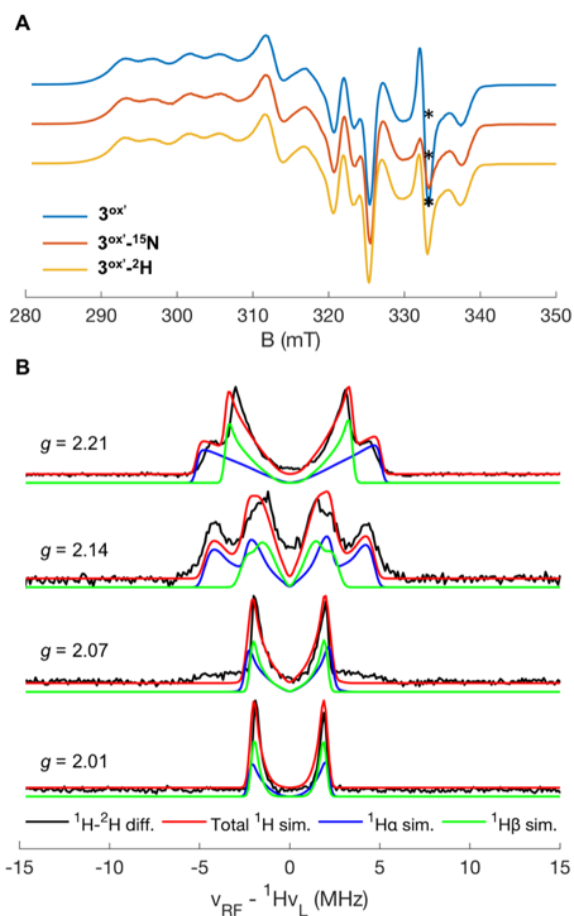**Figure 5.** (A) X-band CW EPR spectra of $\mathbf{3^{ox'}}$, $\mathbf{3^{ox'}}$-^{15}N, $\mathbf{3^{ox'}}$-^{2}H in 2-MeTHF. Acquisition parameters: MW frequency = 9.34 GHz; temperature = 77 K; MW power = 6.5 mW; modulation amplitude = 2 G;

8

conversion time = 82 ms. Asterisks denote the isotropic EPR signals arising from unreacted 2,4,6-tri-*ter*t-butylphenoxyl radical. (B) Field-dependent Q-band Davies ENDOR ^{1}H minus ^{2}H difference spectra of **3$^{ox'}$** and **3$^{ox'}$-^{2}H**. Simulation parameters: **g** = [2.223, 2.084, 2.027]; **A**(^{1}Hα) = [10.3, -5.0, -4.3] MHz, **A**(^{1}Hβ) = [7.0, -4.2, -4.0] MHz. ^{1}H hyperfine tensors rotated ^{1}Hα (α,β,γ)° = (24, 15, 0)° and ^{1}Hβ (α,β,γ)° = (17, 10, 0)° relative to g-tensor frame. Acquisition parameters: MW frequency = 34.039 GHz; MW π pulse length = 80 ns; interpulse delay τ = 240 ns; π_{RF} pulse length = 15 μs; T$_{RF}$ delay = 2 μs; shot repetition time (srt) = 6 ms; temperature = 12 K.
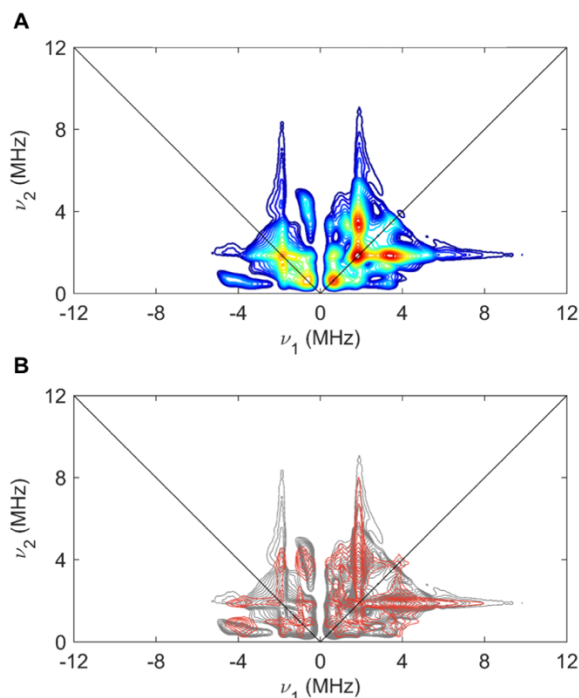

Figure 6. A) X-band ^{14}N HYSCORE spectrum of **3$^{ox'}$** in 2-MeTHF measured at 337.5 mT (g = 2.066). B) Overlay of ^{14}N simulation contours (red) with experimental difference contours (gray). Experimental conditions: microwave frequency = 9.760 GHz; temperature = 12 K; τ = 140 ns, t$_1$ = t$_2$ = 100 ns; Δt$_1$ = Δt$_2$ = 16 ns; shot repetition time (srt) = 1 ms. Simulation parameters: g = [2.223, 2.084, 2.027]; **A**(^{14}N) = ±[-2.57, -0.86, -1.35] MHz; e^2Qq/h = 1.7 MHz; η = 1.0, ^{14}N quadrupole tensor rotated (α,β,γ)° = (-10, 60, 0)° relative to g-tensor frame.

The hyperfine couplings to two distinct classes of hydrogen nuclei were detected through Q-band ^{1}H-^{2}H Davies ENDOR, with **A**(^{1}Hα) = ±[10.3, -5.0, -4.3] MHz and **A**(^{1}Hβ) = ±[7.0, -4.2, -4.0] MHz, (Fig. 5B, see SI for additional pulse EPR data and details). Additionally, hyperfine coupling to two distinct phosphorus nuclei are observed and simulated as **A**(^{31}Pα) = ±[285, 270, 110] MHz, **A**(^{31}Pβ) =

9

±[120, 125, 375] MHz. The hyperfine coupling to nitrogen was determined as $\mathbf{A}(^{14}N) = \pm[-2.57, -0.86, -1.35]$ MHz through a combination of X- and Q-band hyperfine sublevel correlation spectroscopy (HYSCORE) of $\mathbf{3^{ox'}}$ and $\mathbf{3^{ox'}}$-$\mathbf{^{15}N}$ (Figure 6, see SI for additional spectra). In addition to the magnetic hyperfine interaction, the ^{14}N nuclear sublevels are further split by the *electric* interaction of the $I = 1$ ^{14}N nuclear quadrupole with the inhomogeneous electric field induced by electron density in p-orbitals at the nucleus.[35,36] This provides a point-specific measure of the magnitude of the electric field gradient (EFG, parametrized by e^2qQ/h) and its symmetry, with the asymmetry parameter η ranging from η = 0 for pure axial symmetry to η = 1 for full rhombic symmetry. For the ^{14}N nucleus in $\mathbf{3^{ox'}}$, $e^2qQ/h = 1.7$ and η = 1, indicating a fully rhombic EFG. An EFG with η > 0.9 is generally only observed in cases where a lone pair is present at tri-substituted nitrogen in a roughly orthogonal orientation to other bonds, such as in hydrazine and imidazole.[37,38,39] This is incompatible with an axially symmetric terminal amine (-NH$_3$) ligand, which typically exhibit η values near zero, and only range as high as η ≈ 0.4 when one of the amine protons participates in a strong hydrogen bond which breaks this axial symmetry.[40,41,42] Hence, the measured EFG is consistent with the H-bonded adduct of Ni^{III}-NH_2, $\mathbf{3^{ox'}}$, depicted in Eq. 1.

Using the experimental hyperfine values for $\mathbf{3^{ox'}}$ and the corresponding isotopologues, spin density on the amide N is estimated at $|\rho_{N2s}| \approx 0.001$ e$^-$ in the 2s orbital and a sum of $|\rho_{N2p}| < 0.01$ e$^-$ within the three 2p orbitals.[43] Additionally, spin density at the amide protons of $|\rho_{H\alpha}| \approx 0.0007$ e$^-$ and $|\rho_{H\beta}| \approx 0.0008$ e$^-$ are estimated on the two amide-based hydrogen nuclei, respectively.[44] Based on these estimated spin density values, species $\mathbf{3^{ox'}}$ is best described as a Ni-centered metalloradical, rather than a Ni-bound aminyl radical (Fig. 7). For an $S = \frac{1}{2}$, d^7 electronic configuration in an idealized trigonal bipyramidal geometry, the metal-centered spin density is anticipated to reside predominantly in the *xy*-plane (defining the *z*-axis coincident with the C_3-axis).[45] Thus, we suggest that $\mathbf{3^{ox'}}$ is best described by a closed-shell axial Ni–N̈H$_2$ group with an electron hole in the equatorial plane at nickel, with spin leakage onto the equatorial thiolate and phosphine donors.[46] Additional support for this electronic structure description is provided by the extremely high electric field gradient asymmetry (η = 1) at ^{14}N, as determined from the nuclear quadrupole coupling measured via HYSCORE discussed above.

Table 1. EPR simulation parameters for **3ox'** and **6ox**, all hyperfine values are in units of MHz.

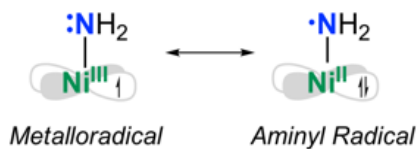|		3ox'		
g	2.223	2.084	2.027	$\Delta g = 0.20$
A(^{14}N)	-2.57	-0.86	-1.35	$|a_{iso}| = 1.6$
A(^{1}Hα)	10.3	-5.0	-4.3	$|a_{so}| = 0.3$
A(^{1}Hβ)	7.0	-4.2	-4.0	$|a_{iso}| = 0.4$
A(^{31}Pα)	285	270	110	$|a_{iso}| = 222$
A(^{31}Pβ)	120	125	375	$|a_{iso}| = 207$
		6ox		
g	2.175	2.070	2.0125	$\Delta g = 0.16$
A(^{14}N)	-4.28	-31.37	-4.28	$|a_{iso}| = 13$
A(^{1}H)	21.5	17.0	6.0	$|a_{so}| = 15$
A(^{31}Pα)	255	220	160	$|a_{iso}| = 212$
A(^{31}Pβ)	175	280	290	$|a_{iso}| = 248$

Figure 7. Resonance structures of **3ox** and **3ox'**, formulated as either a Ni metalloradical or an aminyl radical.
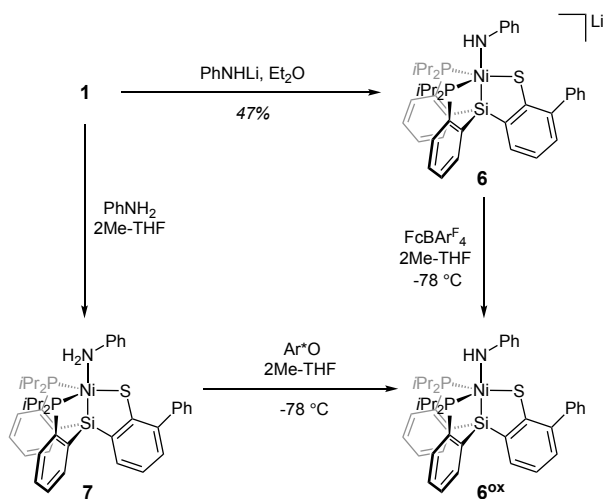
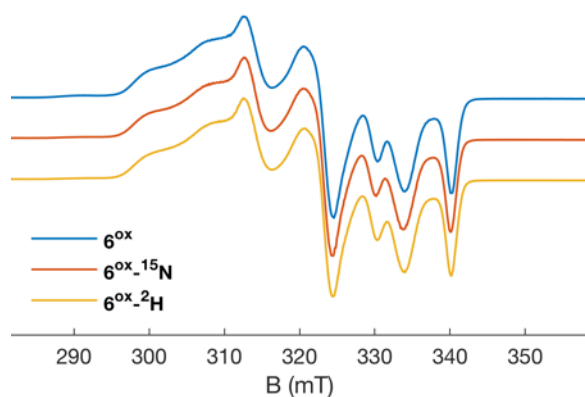**Scheme 2.** Synthesis of compounds **6**, **6ox**, and **7**. Ar*O = 2,4,6-tri-*tert*-butylphenoxyl radical.

Figure 8. (A) X-band CW EPR spectra of 6^{ox}, 6^{ox}-^{15}N, 6^{ox}-^{2}H in 2-MeTHF, generated by hydrogen atom abstraction from the corresponding Ni^{II} aniline adduct. Acquisition parameters: MW frequency = 9.36 GHz; temperature = 77 K; MW power = 6.5 mW; modulation amplitude = 2 G; conversion time = 82 ms.

To obtain spectroscopic data on a stabilized amide derivative, we pursued the synthesis of the corresponding Ni^{III} anilide.[47,48,49] Treatment of **1** with lithium anilide results in the formation of the diamagnetic anilide adduct, [(SiP$_2$S)Ni^{II}(NHPh)]Li (**6**, Scheme 2), which was confirmed by XRD (see SI). Oxidation of **6** with [Cp$_2$Fe][BAr$^F_4$] in 2-MeTHF at -78 °C results in the formation of an S = ½ species as determined by 77 K CW EPR spectroscopy, which is assigned as the neutral anilide complex, (SiP$_2$S)Ni^{III}(NHPh) (**6^{ox}**). Additionally, treatment of the corresponding Ni^{II} aniline species (SiP$_2$S)Ni^{II}(NH$_2$Ph) (**7**) (generated in situ by treatment of **1** with aniline) with 2,4,6-tri-*tert*-butylphenoxyl radical in 2-MeTHF at -78 °C also results in generation of **6^{ox}** via hydrogen atom abstraction, as determined by 77 K CW EPR spectroscopy. For the case of **6^{ox}**, unreacted 2,4,6-tri-*tert*-butylphenoxyl radical is not observed by EPR spectroscopy, and we do not believe there to be a hydrogen bonding interaction between the NHPh group and resulting 2,4,6-tri-*tert*-butylphenol, given that one-electron oxidation of **6** yields an identical EPR spectrum.

The EPR spectrum of **6^{ox}** is well-simulated as a rhombic signal (**g** = [2.175, 2.070, 2.0125]) with coupling to two ^{31}P nuclei (**A**(^{31}Pα) = ±[255, 220, 160] MHz, **A**(^{31}Pβ) = ±[175, 280, 290] MHz, Table 1). Preparation of the ^{15}N- and ^{2}H-labeled analogues (**6^{ox}-^{15}N**, **6^{ox}-^{2}H**) by hydrogen atom abstraction from (SiP$_2$S)Ni^{II}(^{15}NH$_2$Ph) and (SiP$_2$S)Ni^{II}(ND$_2$Ph), respectively, results in similar CW EPR spectra as the natural abundance sample (Fig. 8). Again, a combination of pulse EPR spectroscopies of **6^{ox}**, **6^{ox}-^{15}N**, and **6^{ox}-^{2}H** were utilized to determine hyperfine coupling to an isotopically sensitive nitrogen (**A**(^{14}N) = ±[-4.28, -31.37, -4.28] MHz, see SI) and an isotopically sensitive hydrogen nucleus (**A**(^{1}H) = ±[21.5, 17, 6] MHz, see SI). Based on these hyperfine coupling values, spin density of $|\rho_H| \approx 0.01$ e$^-$ is estimated on the N-*H* hydrogen, and $|\rho_{N2s}| \approx 0.007$ e$^-$ and $|\rho_{N2p}| \approx 0.16$ e$^-$ are estimated on the anilide N.

The gas-phase DFT-optimized structure of 6^{ox} (M06-L, def2tzvp [Ni] and def2svp [all other atoms]) bears a planar NPh fragment, and the spin density map exhibits significant spin delocalization into the phenyl π-system (see SI). These calculated results are suggestive that the spin-bearing nitrogen 2p orbital is in conjugation with the phenyl π-system, which likely contributes to the increased stability of 6^{ox} compared to 3^{ox}. Compared to the hydrogen-bonded $3^{ox'}$, complex 6^{ox} bears more spin density on the nitrogen atom, indicative of greater aminyl character. Relatedly, we posit that the absence of the hydrogen-bonding interaction in 3^{ox} yields enhanced aminyl character compared to $3^{ox'}$. This notion is consistent with 3^{ox} engaging in N-centered radical reactivity to form **2** and **4**, reacting as a "Ni–$\dot{N}H_2$" aminyl species.[50] Gas-phase DFT calculations of 3^{ox} (M06-L, def2tzvp [Ni] and def2svp [all other atoms]) are consistent with such a depiction; a Mulliken spin density of 0.4 e⁻ is estimated on N, and 0.5 e⁻ on Ni (see SI).

Towards the eventual development of a Ni-mediated ammonia oxidation catalyst system, we next explored the possibility of further oxidizing the coordinated hydrazine ligand. Phenoxyl radicals have been used as reagents in stoichiometric and catalytic ammonia oxidation reactions.[3,8bd,51] Accordingly, we were pleased to find that the treatment of the hydrazine adduct **4** with two equivalents of 2,4,6-tri-*ter*t-butylphenoxyl radical generates two equivalents of 2,4,6-tri-*ter*t-butylphenol and the corresponding bridging diazene complex, [(SiP$_2$S)Ni]$_2$(*trans*-N$_2$H$_2$) (**5**, Fig. 2D). This diazene adduct is structurally unusual for a late first-row metal. To the best of our knowledge, there is only one example of a nickel complex featuring a coordinated N$_2$H$_2$ unit, bound side-on to a single Ni center.[52] A Cu$^I_2$(*trans*-N$_2$H$_2$) species related to **5** has also been described.[53] XRD data confirm the assignment of **5** as an end-on bridging diazene and reveal a contracted N–N bond length of 1.277(2) Å compared to hydrazine-bridged **4** (1.488(4) Å). Free diazene bears an N–N bond length of 1.252(2) Å,[54] and hence compound **5** is best described with an intact N–N double bond (HN=NH). By contrast, the aforementioned other example of a Ni-N$_2$H$_2$ species features an elongated N–N bond length of 1.351(3) Å and is described as an HN–NH^{2-} ligand.[52]

In the absence of a radical H-atom abstractor, the hydrazine complex **4** slowly undergoes disproportionation in THF at 25 °C to yield the ammonia adduct **2** and diazene-bridged **5** in a 2:1 molar ratio (Eq. 2). Intermediate species have not been observed in the disproportionation reaction from **4** to **2** and **5**. One possible pathway for this transformation is the concerted transfer of an H$_2$ equivalence between two Ni-bound hydrazine species (e.g. **4** or the mononuclear adduct, (SiP$_2$S)Ni(N$_2$H$_4$)). A related disproportionation reaction was reported for a mononuclear Ru system.[55]

$$\textbf{4} \xrightarrow{\text{THF, 25 °C}} \textbf{2} + ½\,\textbf{5} \qquad (2)$$
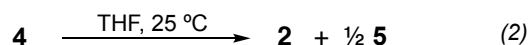
With the aim of regenerating the dinitrogen complex **1** with 2,4,6-tri-*tert*-butylphenoxyl radical, attempts to further oxidize **5** did not prove fruitful. However, treatment of the diazene-bridged species **5** with excess NH_3 in THF results in quantitative displacement of N_2H_2 by NH_3 at nickel, yielding the amine-bound **2**. Free N_2H_2 is unstable toward disproportionation to ½ N_2 and ½ N_2H_4,[56] and hence liberates ammonia-derived N_2 in this system upon displacement from nickel (Scheme 3).[57]
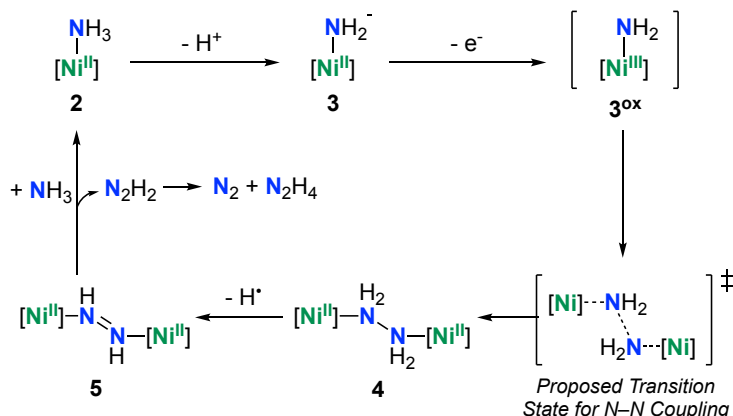
Scheme 3. Stepwise oxidation of NH_3 mediated by $(SiP_2S)Ni$ species.

Diazene displacement from **5** thus closes an overall Ni-mediated ammonia oxidation cycle and regenerates the ammonia adduct **2**. In this stoichiometric cycle, the conversion of 2 NH_3 to ½ N_2 and ½ N_2H_4 constitutes a net $4e^-/4H^+$ process; under potential turnover conditions, the N_2H_4 generated upon diazene disproportionation might in principle undergo further iterative oxidation via hydrazine-bridged **4** and diazene-bridged **5** to achieve the net $6e^-/6H^+$ conversion of 2 NH_3 to N_2. Ongoing studies are directed towards exploring this goal.

CONCLUSION

We have described for the first time a Ni-mediated ammonia oxidation sequence, where the key N–N bond forming step is consistent with homocoupling between two Ni^{III}–NH_2 species to generate a hydrazine-bridged dinickel complex. Reductive elimination of an N–N single bond from a M–NH_2 intermediate has been postulated previously in ammonia oxidation systems, but stoichiometric observation of such reactivity has been lacking. The M–NH_2 homocoupling pathway described here contrasts with mechanisms often invoked for water oxidation catalysis, where high valent metal oxo intermediates are often invoked to precede O–O bond formation.

Akin to catalysts for water oxidation, species that mediate ammonia oxidation may traverse a broad oxidation state range during turnover (e.g. $M^n + NH_3 \rightarrow\rightarrow M^{n+3}\equiv N + 3\ H^{\bullet}$). This is certainly true of some synthetic catalysts that mediate the reverse process of dinitrogen reduction via the distal path-

way.[58] It is thus notable that the ammonia oxidation cycle described herein is carried out between the Ni^{II} and Ni^{III} oxidation states. This narrow redox range is attributable to the fact that the N–N bond forming step can occur from an M–NH$_2$ species (as opposed to a higher valent intermediate featuring a metal-to-nitrogen multiple bond), and that the redox load for H$_2$N–NH$_2$ reductive elimination is distributed between two metal centers. Carrying out multi-electron oxidation processes at a single redox couple (M^n/M^{n+1}) bypasses the need for higher valent intermediates; a conceptually similar paradigm pertains to the alternating mechanism for the reverse nitrogen fixation process.[58] Incorporating these features into the design of ammonia oxidation catalysts provides an attractive strategy for facilitating catalysis using Earth-abundant, late first-row metals.

AUTHOR AFFILIATIONS

Division of Chemistry and Chemical Engineering, California Institute of Technology, Pasadena, California 91125, United States

CORRESPONDING AUTHOR

jpeters@caltech.edu

ORCID

Nina X. Gu: 0000-0002-4637-8418

Paul H. Oyala: 0000-0002-8761-4667

Jonas C. Peters: 0000-0002-6610-4414

COMPETING INTERESTS

The authors declare no competing financial interests.

REFERENCES

[1] (a) Lan, R. & Tao, S. Ammonia as a suitable fuel for fuel cells. *Front. Energy Res.* **2**, 1-4 (2014). (b) Service, R. F. Ammonia – a renewable fuel made from sun, air, and water – could power the globe without carbon. *Science* DOI: 10.1126/science.aau7489 (2018). (c) Klerke, A., Christensen, C. H., Nørskov, J. K., Vegge, T. Ammonia for hydrogen storage: challenges and opportunities. *J. Mater. Chem.* **18**, 2304-2310 (2008).

[2] (a) Zhong, C., Hu, W. B. & Cheng, Y. F. Recent advances in electrocatalysts for electro-oxidation of ammonia. *J. Mater. Chem. A* **1**, 3216-3238 (2013). (b) Chmielarz, L. & Jabłońska, M. Advances in selective catalytic oxidation of ammonia to dinitrogen: a review. *RSC Adv.* **5**, 43408-43431 (2015). (c) Siddharth, K., Chan, Y., Wang, L. & Shao, M. Ammonia electro-oxidation reaction: Recent development in mechanistic understanding and electrocatalyst design. *Curr. Opn.* **9**, 151-157 (2018).

[3] Johnson, S. I., Heins, S. P., Klug, C. M., Wiedner, E. S., Bullock, R. M. & Raugei, S. Design and reactivity of pentapyridyl metal complexes for ammonia oxidation. *Chem. Commun.* **55**, 5083-5086 (2019).

[4] (a) Clarke, R. M. & Storr, T. Tuning Electronic Structure To Control Manganese Nitride Activation. *J. Am. Chem. Soc.* **138**, 15299-15302 (2016). (b) Keener, M., Peterson, M., Hernández Sánchez, R., Oswald, V. F., Wu, G. & Ménard, G. Towards Catalytic Ammonia Oxidation to Dinitrogen: A Synthetic Cycle by Using a Simple Manganese Complex. *Chem. Eur. J.* **23**, 11479-11484 (2017). (c) Würminghausen, T. & Sellmann, D. Cyclo-voltammetrische und präparative untersuchungen zum redoxverhalten der N_2-, N_2H_2-, N_2H_4- und NH_3-komplexe $[C_5H_5Mn(CO)_2]_xL$ MIT x = 1 für L = N_2, N_2H_4, NH_3 und x = 2 für L = N_2H_2. *J. Organomet. Chem.* **1999**, 77-85 (1980). (d) Chantarojsiri, T., Reath, A. H. & Yang, J. Y. Cationic Charges Leading to an Inverse Free-Energy Relationship for N-N Bond Formation by Mn^{VI} Nitrides. *Angew. Chem. Int. Ed.* **57,** 14037-14042 (2018).

[5] (a) Pipes, D. W., Bakir, M., Vitols, S. E., Hodgson, D. J. & Meyer, T. J. Reversible Interconversion between a Nitrido Complex of Os(VI) and an Ammino Complex of Osmium(II). *J. Am. Chem. Soc.* **112**, 5507-5514 (1990). (b) Demadis, K. D., Meyer, T. J. & White, P. S. Localization in *trans,trans*-$[(tpy)(Cl)_2Os^{III}(N_2)Os^{II}(Cl)_2(tpy)]^+$ (tpy = 2,2':6',2''-Terpyridine) *Inorg. Chem.* **36**, 5678-5679 (1997). (c) Buhr, J. D. & Taube, H. Oxidation of $[Os(NH_3)_5CO]^{2+}$ to $[(Os(NH_3)_4CO)_2N_2]^{4+}$. *Inorg. Chem.* **18**, 2208-2212 (1979). (d) Coia, G. M., Devenney, M., White, P. S., Meyer, T. J. & Wink, D. A. Osmium Hydrazido and Dinitrogen Complexes. *Inorg. Chem.* **36**, 2341-2351 (1997).

[6] (a) Ishitani, O., White, P. S. & Meyer, T. J. Formation of Dinitrogen by Oxidation of $[(bpy)_2(NH_3)RuORu(NH_3)(bpy)_2]^{4+}$. *Inorg. Chem.* **35**, 2167-2168 (1996). (b) Ishitani, O., Ando, E. & Meyer, T. J. Dinitrogen Fromation by Oxidative Intramolecular N---N Coupling in *cis,cis*-$[(bpy)_2(NH_3)RuORu(NH_3)(bpy)_2]^{4+}$. *Inorg. Chem.* **42**, 1707-1710 (2003). (c) Collman, J. P., Hutchison, J. E., Lopez, M. A., Guilard, R. & Reed, R. A. Characterization of a Bis-Ammine, a μ_2-Hydrazine, a μ_2-Diazene, and a Remarkably Stable μ_2-Dinitrogen Complex of a Ruthenium Cofacial Diporphyrin. *J. Am. Chem. Soc.* **113**, 2794-2796 (1991). (d) Collman, J. P., Hutchison, J. E., Ennis, M. S., Lopez, M. A. & Guilard, R. Reduced Nitrogen Hydride Complexes of a Cofacial Metallodiporphyrin and Their Oxidative Interconversion. An Analysis of Ammonia Oxidation and Prospects for a Dinitrogen Electroreduction Catalyst Based on Cofacial Metallodiporphyrins. *J. Am. Chem. Soc.* **114**, 8074-8080 (1992).

[7] For a related example of Ru-catalyzed ammonia oxidation to nitrite/nitrate, see: Thompson, M. S. & Meyer, T. J. Oxidation of Coordinated Ammonia to Nitrate. *J. Am. Chem. Soc.* **103**, 5577-5579 (1981).

[8] (a) Habibzadeh, F., Miller, S. L., Hamann, T. W., Smith III, M. R. Homogenous electrocatalytic oxidation of ammonia to N_2 under mild conditions. *Proc. Natl. Acad. Sci.* **116**, 2849-2853 (2019). (b) Bhattacharya, P., Heiden, Z. M., Chambers, G. M., Johnson, S. I., Bullock, R. M. & Mock, M. T. Catalytic Ammonia Oxidation to Dinitrogen by Hydrogen Atom Abstraction. *Angew. Chem. Int. Ed.* **58**, 11618-11624 (2019). (c) Nakajima, K., Toda, H., Sakata, K. & Nishibayashi, Y. Ruthenium-catalysed oxidative conversion of ammonia to dinitrogen. *Nat. Chem.* **11**, 702-709 (2019). (d) Dunn, P., Johnson, S. I., Kaminsky, W. & Bullock, R. M. Diversion of Catalytic C-N Bond Formation to Catalytic Oxidation of NH_3 Through Modification of the Hydrogen Atom Abstractor. *J. Am. Chem. Soc.* **142**, 3361-3365 (2020).

[9] Zott, M. D., Garrido-Barros, P. & Peters, J. C. Electrocatalytic Ammonia Oxidation Mediated by a Polypyridyl Iron Catalyst. *ACS Catal.* **9**, 10101-10108 (2019).

[10] (a) Duan, L, Bozoglian, F., Mandal, S., Stewart, B., Privavlov, T., Llobet, A. & Sun, L. A molecular ruthenium catalyst with water-oxidation activity comparable to that of photosystem II. *Nat. Chem.* **4**, 418-423 (2012). (b) Fillol, J. L., Codolà, Z., Garcia-Bosch, I., Gómez, L., Pla, J. J. & Costas, M. Efficient water oxidation catalysts based on readily available iron coordination complexes. *Nature Chem.* **3**, 807-813 (2011). (c) Concepcion, J. J., Jurss, J. W., Templeton, J. L. & Meyer, T. J. One Site is Enough. Catalytic Water Oxidation by $[Ru(tpy)(bpm)(OH_2)]^{2+}$ and $[Ru(tpy)(bpz)(OH_2)]^{2+}$. *J. Am. Chem. Soc.* **130**, 16462-16463 (2008).

[11] (a) Kärkäs, M. D.,Verho, O., Johnston, E. V. & Åkermark, B. Artificial Photosynthesis: Molecular Systems for Catalytic Water Oxidation. *Chem. Rev.* **114**, 11863-12001 (2014). (b) Blakemore, J. D., Crabtree, R. H. & Brudvig, G. W. Molecular Catalysts for Water Oxidation. *Chem. Rev.* **23**, 12974-13005 (2015).

[12] In contrast, for a relevant example consistent with photochemical HO-OH reductive elimination from a $Ru(OH)_2$ species, see: Kohl, S. W., Weiner, L., Schwartsburd, L., Konstantinovski, L., Shimon, L. J. W., Ben-David, Y., Iron, M. A. & Milstein, D. Consecutive Thermal H_2 and Light-Induced O_2 Evolution from Water Promoted by a Metal Complex. *Science* **324**, 74-77 (2009).

[13] Betley, T. A. & Peters, J. C. A Tetrahedrally Coordinated L_3Fe-N_x Platform that Accommodates Terminal Nitride (Fe^{IV}⋮N) and Dinitrogen ($Fe^I-N_2-Fe^I$) Ligands. *J. Am. Chem. Soc.* **126**, 6252-6254 (2004).

[14] (a) Mankad, N. P., Müller, P. & Peters, J. C. Catalytic N-N Coupling of Aryl Azides to Yield Azoarenes via Trigonal Bipyramid Iron-Nitrene Intermediates. *J. Am. Chem. Soc.* **132**, 4083-4085 (2010). (b) Powers, I. G., Andjaba, J. M., Luo, X., Mei, J. & Uyeda, C. Catalytic Azoarene Synthesis from Aryl Azides Enabled by a Dinuclear Ni Complex. *J. Am. Chem. Soc.* **140**, 4110-4118 (2018). (c) Yiu, S.-M., Lam, W. W. Y., Ho, C.-M., Lau, T.-C. Facile N⋯N Coupling of Manganese(V) Imido Species. *J. Am. Chem. Soc.* **129**, 803-809 (2007).

[15] Coia, G. M., White, P. S., Meyer, T. J., Wink, D. A., Keefer, L. K. & Davis, W. M. Preparation of Osmium Hydrazido Complexes by Interception of an Osmium(IV) Imido Intermediate. *J. Am. Chem. Soc.* **116**, 3649-3650 (1994).

[16] Su, Q.-Q., Fan, K., Huang, X.-D., Xiang, J., Cheng, S.-C., Ko, C.-C., Zheng, L.-M., Kurmoo, M. & Lau, T.-C. Field-induced slow magnetic relaxation in low-spin $S = ½$ mononuclear osmium(v) complexes. *Dalton Trans.* **49**, 4084-4092 (2020).

[17] (a) Diccianni, J. B., Hu, C. & Diao, T. N-N Bond Forming Reductive Elimination via a Mixed-Valent Nickel(II)-Nickel(III) Intermediate. *Angew. Chem. Int. Ed.* **55**, 7534-7538 (2016). (b) Kosobokov, M. D.. Sandleben, A., Vogt, N., Klein, A. & Vicic, D. A. Nitrogen-Nitrogen Bond Formation via a Substrate-Bound Anion at a Mononuclear Nickel Platform. *Organometallics* **37**, 521-525 (2018).

[18] For examples of aryl diazene (ArN=NAr) formation proposed to occur via initial N-N single-bond coupling between M-NHAr species, see (a) Gephart III, R. T., Huang, D. L, Aguila, M. J. B., Schmidt, G., Shahu, A. & Warren, T. H. Catalytic C-H Amination with Aromatic Amines. *Angew. Chem. Int. Ed.* **51**, 6488-6492 (2012). (b) Kinoshita, K. On the Mechanism of. Oxidation of Cuprous Chloride, Pyridine and Air. II. The Mechanism of Formation of Azobenzene from Aniline. *Bull. Chem. Soc. Jpn.* **32**, 780-783 (1959). (c) Bakhoda, A. G., Wiese, S., Greene, C., Figula, B. C., Bertke, J. A. & Warren, T. H. Radical Capture at Nickel(II) Complexes: C-C, C-N, and C-O Bond Formation. *Organometallics* **39**, 1710-1718 (2020).

[19] (a) Ryan, M. C., Kim, Y. J., Gerken, J. B., Wang, F., Aristov, M. M., Martinelli, J. R. & Stahl, S. S. Mechanistic insights into copper-catalyzed aerobic oxidative coupling of N-N bonds. *Chem. Sci.* **11**, 1170-1175 (2020). (b) Pearce, A. J., Harkins, R. P., Reiner, B. R., Wotal, A. C., Dunscomb, R. J. & Tonks, I. A. Multicomponent Pyrazole Synthesis from Alkynes, Nitriles, and Titanium Imido Complexes via Oxidatively Induced N-N Bond Coupling. *J. Am. Chem. Soc.* **142**, 4390-4399 (2020). (c) Wang, F., Gerken, J. B., Bates, D. M., Kim, Y. J. & Stahl, S. S. Electrochemical Strategy for Hydrazine Synthesis: Development and Overpotential Analysis of Methods for Oxidative N-N Coupling of an Ammonia Surrogate. *J. Am. Chem. Soc.* **142**, 12349-12356 (2020).

[20] (a) Saouma, C. T. & Peters, J. C. M≡E and M=E complexes of iron and cobalt that emphasize three-fold symmetry (E = O, N, NR). *Coord. Chem. Rev.* **255**, 920-937 (2011). (b) Ray, K., Heims, F. & Pfaff, F. F. Terminal Oxo and Imido Transition-Metal Complexes of Groups 9-11. *Eur. J. Inorg. Chem.* 3784-3807 (2013).

[21] Gu, N. X., Oyala, P. H. & Peters, J. C. An $S = ½$ Iron Complex Featuring N_2, Thiolate, and Hydride Ligands: Reductive Elimination of H_2 and Relevant Thermochemical Fe-H Parameters. *J. Am. Chem. Soc.* **140**, 6374-6382 (2018).

[22] Gu, N. X., Oyala, P. H. & Peters, J. C. H$_2$ Evolution from a Thiolate-Bound Ni(III) Hydride. *J. Am. Chem. Soc.* **142**, 7827-7835 (2020).

[23] Complex **1** is isolated as a dinickel species featuring a bridging N$_2$ unit, but is in equilibrium with the monomeric (SiP$_2$S)NiN$_2$ in solution under an N$_2$ atmosphere.

[24] Crystals of the sodium analogue, [(SiP$_2$S)Ni^{II}(NH$_2$)]Na(THF)$_3$, can be grown from THF/pentane mixtures, and XRD data reveal the coordination of three THF molecules to the sodium ion. ^{1}H NMR data of [(SiP$_2$S)Ni^{II}(NH$_2$)]Na(THF)$_3$ in C$_6$D$_6$ also corroborate the presence of three THF molecules.

[25] (a) Cámpora, J., Palma, P., del Río, D., Conejo, M. M. & Álvarez, E. Synthesis and Reactivity of a Mononuclera Parent Amido Nickel Complex. Structures of Ni[C$_6$H$_3$-2,6-(CH$_2$P^{i}Pr$_2$)$_2$](NH$_2$) and Ni[C$_6$H$_3$-2,6-(CH$_2$P^{i}Pr$_2$)$_2$](OMe). *Organometallics* **23**, 5653-5655 (2004). (b) Adhikari, D., Mossin, S., Basuli, F., Dible, B. R., Chipara, M., Fan, H., Huffman, J. C., Meyer, K. & Mindiola, D. J. A Dinuclear Ni(I) System Having a Diradical Ni$_2$N$_2$ Diamond Core Resting State: Synthetic, Structural, Spectroscopic Elucidation, and Reductive Bond Splitting Reactions. *Inorg. Chem.* **47**, 10479-10490 (2008). (c) Gutsulyak, D. V., Piers, W. E., Borau-Garcia, J. & Parvez, M. Activation of Water, Ammonia, and Other Small Molecules by PC$_{carbene}$P Nickel Pincer Complexes. *J. Am. Chem. Soc.* **135**, 11776-11779 (2013). (d) Schmeier, T. J., Nova, A., Hazari, N. & Maseras, F. Synthesis of PCP-Supported Nickel Complexes and their Reactivity with Carbon Dioxide. *Chem. Eur. J.* **18**, 6915-6927 (2012). (e) Yoo, C. & Lee, Y. A T-Shaped Nickel(I) Metalloradical Species. *Angew. Chem. Int. Ed.* **56**, 9502-9506 (2017). (f) Mousa, A. H., Bendix, J. & Wendt, O. F. Synthesis, Characterization, and Reactivity of PCN Pincer Nickel Complexes. *Organometallics* **37**, 2581-2593 (2018).

[26] Oxidation reactions of **3** are performed in a glovebox coldwell externally cooled with a dry ice/acetone bath.

[27] Creutz, S. E. & Peters, J. C. Exploring secondary-sphere interactions in Fe-N$_x$H$_y$ complexes relevant to N$_2$ fixation. *Chem. Sci.* **8**, 2321-2328 (2017).

[28] Kohata, K., Fukuyama, T. & Kuchitsu, K. Molecular Structure of Hydrazine As Studied by Gas Electron Diffraction. *J. Phys. Chem.* **86**, 602-606 (1982).

[29] The ^{1}H NMR spectrum of the oxidation reaction of [(SiP$_2$S)Ni^{II}(ND$_2$)]Li bears a minor component of the hydrazine adduct with N-^{1}H bonds, which is expected due to incomplete deuteration of the starting ^{2}H-labeled amide.

[30] EPR samples were prepared by mixing 2-MeTHF solutions of **3** and [Cp$_2$Fe][BAr$^F_4$] (0.8 equiv.) at -78 ºC, followed by immediate freezing in liquid N$_2$. However, samples prepared by this method exhibited no EPR-active species by 77 K CW EPR spectroscopy. Alternatively, an EPR tube containing a frozen 2-MeTHF solution of [Cp$_2$Fe][BAr$^F_4$] (0.8 equiv.) layered over a frozen 2-MeTHF solution of **3** was allowed to thaw, and the layers were mechanically mixed at *ca.* -135 ºC. (See Ref. 31 for details regarding EPR sample preparation via mechanical mixing at *ca.* -135 ºC). Analysis of this sample by 77 K CW EPR spectroscopy revealed a weak S = ½ EPR signal that matches the spectrum observed upon one-electron oxidation of **2** with [Cp$_2$Fe][BAr$^F_4$] at -78 ºC, likely arising from [(SiP$_2$S)Ni^{III}(NH$_3$)] [BAr$^F_4$]. It is likely that upon transient generation of **3^{ox}**, hydrogen atom abstraction from solvent is still facile at these low temperatures, and a minor portion of the resulting amine-species **2** undergoes additional oxidation during mixing to yield the observed [(SiP$_2$S)Ni^{III}(NH$_3$)][BAr$^F_4$].

[31] Anderson, J. S., Cutstail, G. E., Rittle, J., Connor, B. A., Gunderson, W. A., Zhang, L., Hoffman, B. M. & Peters, J. C. Characterization of an Fe≡N-NH$_2$ Intermediate Relevant to Catalytic N$_2$ Reduction to NH$_3$. *J. Am. Chem. Soc.* **137**, 7803-7809 (2015).

[32] Regarding the metalloradical generated by **2** and 2,4,6-tri-*tert*-butylphenoxyl radical, a possible alternative assignment is the six-coordinate Ni-bound aryloxide adduct, (SiP$_2$S)Ni^{III}(NH$_3$)(OAr). However, given that the ^{1}H-^{2}H ENDOR data are well-simulated with coupling to just two isotopically sensitive hydrogen nuclei (rather than three), the fully rhombic symmetry of the ^{14}N EFG as measured by HYSCORE, combined with the considerable steric profile of the phenoxyl radical, we disfavor this assignment. Furthermore, the g values and ^{31}P hyperfine coupling parameters of the metalloradical are comparable to that of other five-coordinate (SiP$_2$S)Ni^{III}-X species (as described in the main text), which additionally disfavor this six-coordinate aryloxide adduct assignment.

[33] The UV-vis spectrum of the related Ni^{III} methyl species, (SiP$_2$S)Ni^{III}-Me, exhibits transitions at 635 nm and 925 nm.

[34] Of note, the relative intensities of the phenoxy radical and **3$^{ox'}$** in Fig. 5A are not representative of the speciation in the sample; the phenoxyl radical signal is saturated at the microwave power levels which the EPR spectra are collected (6.5 mW), which results in decreased observed intensity of the phenoxyl radical signal. See the Support-

ing Information for an EPR spectrum collected at 8.7 µW, where saturation behavior is not observed for the phenoxyl radical.

[35] Das, T. P. H.; E. L. *Nuclear quadrupole resonance spectroscopy*; Academic Press: New York (1958).

[36] Lucken, E. A. C. *Nuclear Quadrupole Coupling Constants*; Academic Press: London (1969).

[37] Edmonds, D. T. & Summers, C. P. ^{14}N Pure Quadrupole Resonance in Solid Amino Acids. *Journal of Magnetic Resonance.* **12**, 134-142 (1973).

[38] Ikeda, R. S., Noda, S., Nakamura, D. & Kubo, M. Nuclear quadrupole resonance of ^{14}N in hydrazine derivatives. *Journal of Magnetic Resonance.* **5**, 54-62 (1971).

[39] Hunt, M. J., Mackay, A. L. & Edmonds, D. T. Nuclear quadrupole resonance of ^{14}N in Imidazole and Related Compounds. *Journal of Magnetic Resonance.* **9**, 66 (1975).

[40] Sasane, A. & Smith, J. A. S. ^{14}N quadrupole resonance in carbonatotetramminecobalt(III) bromide. *Journal of Magnetic Resonance.* **32**, 265-287 (1978).

[41] Oyala, P. H., Stich, T. A., Debus, R. J. & Britt, R. D. Ammonia binds to the dangler manganese of the photosystem II oxygen-evolving complex. *J. Am. Chem. Soc.* **137**, 8829-8837 (2015).

[42] Marchiori, D. A., Oyala, P. H., Debus, R. J., Stich, T. A. & Britt, R. D. Structural Effects of Ammonia Binding to the Mn_4CaO_5 Cluster of Photosystem II. *J. Phys. Chem. B.* **122**, 1588-1599 (2018).

[43] The spin density in the ^{14}N 2s orbital was estimated by scaling the isotropic hyperfine coupling (a_{iso}; $\mathbf{A} = [A_x, A_y, A_z]$, $a_{iso} = (A_x + A_y + A_z)/3$) of the ^{14}N nuclei by the calculated a_{iso} value for unit spin density in a nitrogen 2s orbital (1811 MHz). The dipolar tensors ($\mathbf{T}$; $\mathbf{A} = a_{iso} + \mathbf{T}$) for an electron fully localized in each of the ^{14}N 2p orbitals are defined as $\mathbf{T^0}(2p_x) = [111.0, -50.5, -50.5]$ MHz, $\mathbf{T^0}(2p_y) = [-50.5, 111.0, -50.5]$ MHz, $\mathbf{T^0}(2p_z) = [-50.5, -50.5, 111.0]$. The upper bound on spin density in the ^{14}N 2p orbitals for $\mathbf{3^{ox}}$ was estimated by decomposing the measured dipolar tensor by $\mathbf{T^0}(2p_x)$, $\mathbf{T^0}(2p_y)$, and $\mathbf{T^0}(2p_z)$. See: Morton, J. R. & Preston, K. F. Atomic Parameters for Paramagnetic Resonance Data. *J. Magn. Reson.* **30**, 577-582 (1978).

[44] The spin density on the $^1H\alpha$ and $^1H\beta$ nuclei were estimated by scaling the isotropic hyperfine coupling (a_{iso}; $\mathbf{A} = [A_x, A_y, A_z]$, $a_{iso} = (A_x + A_y + A_z)/3$) of those two hydrogens by the a_{iso} value for a free hydrogen atom (1420 MHz; see: Wittke, J. P. & Dicke, R. H. Redetermination of the Hyperfine Splitting in the Ground State of Atomic Hydrogen. *Phys. Rev.* **103**, 620−631 (1956)).

[45] Gunderson, W. A., Suess, D. L. M., Fong, H., Wang, X., Hoffmann, C. M., Cutsail III, G. E., Peters, J. C. & Hoffman, B. M. Free H_2 Rotation vs Jahn-Teller Constraints in the Nonclassical Trigonal (TPB)Co-H_2 Complex. *J. Am. Chem. Soc.* **136**, 14998-15009 (2014).

[46] Of note, the EPR parameters of $\mathbf{3^{ox'}}$ are also similar to those obtained for the reported methyl analogue, $(SiP_2S)Ni^{III}$–Me (**8**, see Ref. 22). The 77 K CW EPR spectrum of **8** is well-simulated as a rhombic signal (**g** = [2.255, 2.073, 2.037]) with coupling to two ^{31}P nuclei ($\mathbf{A}(^{31}P\alpha) = \pm[260, 257, 130]$ MHz, $\mathbf{A}(^{31}P\beta) = \pm[170, 133, 330]$ MHz, Table 1). XRD data on complex **8** confirm a trigonal bipyramidal geometry at Ni. Consistent with the simplified MO description detailed above, the reported DFT-calculations of **8** (M06-L, def2tzvp [Ni] and def2svp [all other atoms]) indicate minimal spin leakage onto the methyl group (-0.002 e$^-$ (C); 0.002 e$^-$ ($\Sigma\rho_{3H}$)) and assign almost all of the Mulliken spin density in the equatorial xy plane (0.65 e$^-$ (Ni); 0.10, 0.04 e$^-$ (2P); 0.19 e$^-$ (S); $\Sigma\rho_{Ni,2P,S} = 0.98$ e$^-$). Furthermore, the calculated spin density plot shows that the unpaired spin on Ni resides in the equatorial xy plane. The comparable *g* values and ^{31}P hyperfine coupling values of $\mathbf{3^{ox'}}$ and **8** are consistent with similar electronic structures between the two species.

[47] We have also pursued the characterization of related $(SiP_2S)NiNR_2$ (R = Me, SiMe₃) species as models, but to date without success.

[48] For examples of characterized Ni(III) complexes featuring ligation to terminally-bound, substituted amides (Ni^{III}-NRR'), see: (a) Kochem, A., Gellon, G., Leconte, N., Baptite, B., Philouze, C., Jarjayes, O., Orio, M. & Thomas, F. Stable Anilinyl Radicals Coordinated to Nickel: X-ray Crystal Structure and Characterization. *Chem. Eur. J.* **19**, 16707-16721 (2013). (b) Hanss, J. & Krüger, H.-J. First Isolation and Structural Characterization of a Nickel(III) Complex Containing Aliphatic Thiolate Donors. *Angew. Chem. Int. Ed.* **37**, 360-363 (1998). (c) Tripathi, A., Syal, R. K. & Bharadwaj, P. K. An air-stable Ni(III) complex with thiolate, phenolate and amide ligation. *Polyhedron* **18**, 2229-2232 (1999). (d) Collins, T. J, Nichols, T. R. & Uffelman, E. S. A Square-Planar Nickel(III) Complex of an Innocent Ligand System. *J. Am. Chem. Soc.* **113**, 4708-4709 (1991). (e) Patra, A. K. & Mukherjee, R. Bivalent, Trivalent, and Tetravalent Nickel Complexes with a Common Tridentate Deprotonated Pyridine Bis-

Amide Ligand. Molecular Structures of Nickel(II) and Nickel(IV) and Redox Activity. *Inorg. Chem.* **38**, 1388-1393 (1999). (f) Singh, A. K. & Mukherjee, R. Structure and properties of bivalent nickel and copper complexes with pyrazine-amide-thioether coordination stabilization of trivalent nickel. *Dalton Trans.* 2886-2891 (2005).

[49] For related examples of Ni(I) arylamide species, see: (a) Mindiola, D. J. & Hillhouse, G. L. Terminal Amido and Imido Complexes of Three-Coordinated Nickel. *J. Am. Chem. Soc.* **123**, 4623-4624 (2001). (b) Laskowski, C. A. & Hillhouse, G. L. Two-Coordinate d^9 Complexes. Synthesis and Oxidation of NHC Nickel(I) Amides. *J. Am. Chem. Soc.* **130**, 13846-13847 (2008).

[50] For examples of characterized metal-bound aminyl radicals, see: (a) Büttner, T., Geier, J., Frison, G., Harmer, J., Calle, C., Schweiger, A., Schönberg, H. & Grützmacher. A Stable Aminyl Radical Metal Complex. *Science* **307**, 235-238 (2005). (b) Mankad, N. P., Antholine, W. E., Szilagyi, R. K. & Peters, J. C. Three-Coordinate Copper(I) Amido and Aminyl Radical Complexes. *J. Am. Chem. Soc.* **131**, 3878-3880 (2009). (c) Adhikari, D., Mossin, S., Basuli, F., Huffman, J. C., Szilagyi, R. K., Meyer, K. & Mindiola, D. J. Structural, Spectroscopic, and Theoretical Elucidation of a Redox-Active Pincer-Type Ancillary Applied in Catalysis. *J. Am. Chem. Soc.* **130**, 3676-3682 (2008). (d) Hicks, R. G. Metal Complexes of Aminyl Radicals. *Angew. Chem. Int. Ed.* **47**, 7393-7395 (2008). (e) Suarez, A. I. O., Lyaskovskyy, V., Reek, J. N. H., van der Vlugt, J. I. & de Bruin, B. Complexes with Nitrogen-Centered Radical Ligands: Classification, Spectroscopic Features, Reactivity, and Catalytic Applications. *Angew. Chem. Int. Ed.* **52**, 12510-12529 (2013).

[51] (a) Bhattacharya, P., Heiden, Z. M., Wiedner, E. S., Raugei, S., Piro, N. A., Kassel, W. S., Bullock, R. M. & Mock, M. T. Ammonia Oxidation by Abstraction of Three Hydrogen Atoms from a Mo-NH_3 Complex. *J. Am. Chem. Soc.* **139**, 2916-2919 (2017). (b) Cook, B. J., Johnson, S. I., Chambers, G. M., Kaminsky, W. & Bullock, R. M. Triple hydrogen atom abstractions from Mn-NH_3 complexes results in cyclophosphazenium cations. *Chem. Commun.* **55**, 14058-14061 (2019).

[52] Köthe, C., Braun, B., Herwig, C. & Limberg, C. Synthesis, Characterization, and Interconversion of β-Diketiminato Nickel N_xH_y Complexes. *Eur. J. Inorg. Chem.* 5296-5303 (2014).

[53] The $Cu^I_2(trans$-$N_2H_2)$ species is structurally characterized, but the determination of reliable bond metrics of the N_2H_2 fragment was hindered by crystal disorder. However, the methylated $Cu^I_2(trans$-$N_2(CH_3)_2)$ derivative exhibits a crystallographically determined N-N bond length of 1.27(2) Å, comparable to that of **5**. See: Fujisawa, K., Lehnert, H., Ishikawa, Y. & Okamoto, K. Diazene Complexes of Copper: Synthesis, Spectroscopic Analysis, and Electronic Structure. *Angew. Chem. Int. Ed.* **43**, 4944-4947 (2004).

[54] Carlotti, M., Johns, J. W. C. & Trombetti, A. The ν_5 Fundamental Bands of N_2H_2 and N_2D_2. *Can. J. Phys.* **52**, 340-344 (1974).

[55] Sellmann, D., Hille, A., Rösler, A., Heinemann, F. W., Moll, M., Brehm, G., Schneider, S., Reiher, M., Hess, B. A. & Bauer, W. Binding N_2, N_2H_2, N_2H_4, and NH_3 to Transition-Metal Sulfur Sites: Modeling Potential Intermediates of Biological N_2 Fixation. *Chem. Eur. J.* **10**, 819-830 (2004).

[56] Stanbury, D. M. Kinetic Behavior of Diazene in Aqueous Solution. *Inorg. Chem.* **30**, 1293-1296 (1991).

[57] Upon quenching the reaction mixture with excess HCl, 0.4 equivalents of hydrazine (in the form of N_2H_5Cl) per **5** were detected in the mixture. Additionally, when this reaction is performed under an argon atmosphere, 0.5 equivalents of dinitrogen per **5** were detected in the headspace, see Supporting Information for additional details.

[58] Chalkley, M. J., Drover, M. W. & Peters, J. C. Catalytic N_2-to-NH_3 (or -N_2H_4) Conversion by Well-Defined Molecular Coordination Complexes. *Chem. Rev.* **120**, 5582-5636 (2020).

TOC GRAPHIC